HITUBES PROJECT

DESIGN AND INTEGRITY ASSESSMENT OF HIGH STRENGTH TUBULAR STRUCTURES FOR EXTREME LOADING CONDITIONS

Deliverables 7.1, 7.2 & 7.3 – Design guidelines and time dependent reliability assessment

D7.1: Report on design guidelines and recommendations for HSS for tubular structures
D7.2: Report on design guidelines and recommendations for tubular members and connections
D7.3: Report on maintenance and durability of HSS tubular structures

Authors

Sergio Rivera, Ricardo Alvarez, Ricardo Lezcano
Eva Johansson, Nuria Fuertes
Giuseppe Demofonti, Giuliana Zilli, Gian Marco Tamponi, Jan Ferino
Helena Guvaia, Carlos Maia
Jean-Pierre Jaspart, Jean-François Demonceau, Long Van Hoang, Ly Dong Phuong Lam
Spyros Karamanos , Philip Perdikaris, Aglaia Pournara, Charis Papatheocharis, George Varelis
Oreste S. Bursi, Anil Kumar

Contributing Partners

Fundacion ITMA, Spain
Korrosions Och Metallforskningsinstitutet AB, Sweden
Centro Sviluppo Materiali, Italy
Instituto de Soldadura e Qualidade, Portugal
Université de Liège, Belgium
University of Thessaly, Greece
University of Trento, Italy

Table of Contents

D.7.1. Report on design guidelines and recommendations for HSS for tubular structures method

The design and application issues of HSS in bridge structures are reported herein.

D.7.1.1. Design of bridges with high strength steel

Bridge design with S460 and S690 steel is not fundamentally different with the conventional steel (S355) commonly used nowadays [1].

If some special bridges: mobile, temporary or pedestrian can be built completely with S460 steel or even S690, things are different for road bridges where the technical options chosen by designers for fatigue justifications are a combination of two steel grades S355 and S460.

Many modern bridges built in France and Germany have been designed with these particularities. However in rail bridges, these high grade steels are completely absent, because these bridges are designed for stiffness.

Design detailing can be classified in two main groups:

- Main structural elements
- Structural detail elements

In the main structural design of decks, the different steel grades have to be distributed longitudinally and sometimes transversely. Structural detail points concern local elements with high stress values, for example supports elements, piers or pylons.

The opportunity to include high strength steel in conventional bridge design depends on the bridge structure: long pr small span decks, steelworks with plate girders, truss or hollow-tubular sections.

These steels allow a reduction of steel sections, hence smaller weights, reduction in thickness and in welds at end to end joints of continuous girders.

This aspect tends to show that there are only advantages to use high strength steel for bridges; however attention should be paid to the following points:

- Maintain a minimal stiffness to respect the deflection limits under service conditions,
- Ensure buckling and other stability which are independent of the yield strength,
- Resistance to fatigue which is also independent of the yield strength,
- Toughness against brittle fracture.

Stiffness can be increased by increasing the composite action with concrete, for example double composite action with concrete at the lower flanges also.

In order to maintain a good resistance to buckling, it is often preferable to have thicker webs in a lower steel grade. The design of this type of hybrid girders is now well defined in different parts of EN 1993. Fatigue resistance can be increased with post weld treatments like grinding, thermal dressing of the weld or peening.

D.7.1.2. High-strength high-performance steel for long span bridges

The benefits and the limitations of the use of high-strength high-performance steel for conventional bridge types are well documented. However, the use of higher strength steel for cable supported long span steel bridges is still emerging. There are several key differences in the behavior of cable-supported long span structures that makes the design optimization of these quite different from those of girder and truss type bridges. These same differences make high-strength high-performance steel an ideal material of application on these longer span structures. While these advantages make them even more suitable for long span applications, they are yet to be fully exploited for these types of signature large-scale structures [2].

For example, the traditional live load deflection control of conventional bridge types requires stiffer girders, or heavier sections. The uses of higher strength steels produce more flexible cross sections that produce higher live load deflections. While live load deflection as a design criterion is under review and may change in the future, this limits the realization of maximum potential benefits of the higher strength steels for conventional bridges. Higher strength steel girders have higher strength to stiffness ratio (F/E)

than the traditional grade 50 steels. While this can be a disadvantage in conventional bridge design due to deflection control, it is very desirable for cable-supported bridges due to the following two factors.

First, the stiffness of long span cable-supported structural systems is less dependent on the stiffness of the superstructure, especially for gravity type loading conditions. The controlling live load deflections of long span structures are produced by global loading conditions involving longer length lane loads. While these deflections are highly dependent on the tower stiffness and the stiffness of the supporting cable system, they can be shown to be practically independent of the superstructure stiffness in the range of girder depths used in typical applications.

Second, the internal moments produced in long span bridge superstructures are due to deformations produced by the global loading. Thus the stiffer girder produces higher demand leading to needing a larger girder that in turn increases the demand. The use of high-strength high-performance steel provides a means of increasing capacity without measuring stiffness and can provide tremendous advantages for long span bridges. This is a factor not recognized widely at the present time and it is hoped that a discussion on this topic would bring it the attention it deserve.

Furthermore, as evident by the Charles River Bridge in Bostan, MA, high-strength high-performance steel can be the material of choice for special applications on long span bridges. This first time application took advantage of high-strength high-performance steel for its steel composite tower and all of the cable anchorages. The design provided optimal solutions considering the complex design issues, improving constructability and the visual aspects of some key components. This proved to be, while a-typical, an interesting application of this material in its early stages of its availability in the US. Many of the fabrication aspects were first-time applications that required thorough investigation to establish the feasibility early in the design process.

D.7.1.3. References

[1] Hoorpah W., Vigo J.M., “Innovative design of bridges with high strength steel,” in 7th International Conference on Steel Bridges, 2008.

[2] Gunther Hans-Peter et al., “SED 8: Use and application of high-performance steels for steel structures,” IABSE, 2005.

D.7.2. Report on design guidelines and recommendations for tubular members and connections

D.7.2.1 Design guidelines and recommendations for welded connections

In welded tubular connections, failure usually occurs in the form of cracks at a discontinuity or stress raiser, associated with a microscopic defect at the weld toe. As a result, the cracks (under monotonic or fatigue loading) initiate at these locations irrespective of the steel grade. Higher grades of steel can be used, they improve the static strength of the joints, but do not necessarily improve the deformation capacity or the fatigue strength.

Welding Details, Procedures and Improvement Methods in Tubular Joints

CIDECT Design Guides No. 1 and 8 present typical weld details at the main locations of welded tubular connections constructed with circular hollow sections. More extensive information on the detailing of those joints can be found in the AWS Welding Code. Weld start/stop positions for non-continuous welds should not be located at points of high stress concentration (crown and saddle points), since these can themselves cause stress concentrations.

Fatigue behavior improvement of weld joints

Welding results in residual stresses due to material cooling which value is about the same of the yield strength of the weld metal. In the toe of the weld there are three discontinuities present at the same time and local. There is a metallurgical discontinuity between parent metal and weld metal structures, discontinuity in stress levels and geometrical discontinuity. This combination affects the local fatigue behavior.

Various methods of improving the fatigue resistance of welded connections are available. Mechanical penning mainly introduces compression stresses in the toe of the weld that will reduce the balance of tensile stresses resulting from external actions. Mechanical penning can be applied by using sand blasting, hammer needle and UIT. UIT (ultrasonic impact treatment), used in the project, introduces both compressive stresses and also increases the toe radius). The application of a rotating burin is also used to obtain a small rounded groove in the weld toe Also Laser re-melting or TIG dressing of the weld toe are available and are proficient in smothering the transition of the weld to parent metal. Metallographic analyses of hardness and eventual temper structures should be performed prior to application of these two last methods. These welding methods should be considered as weld repairs which need a qualification of the welding procedures specifications before use.

Impacts

In WP4.1 it was observed lower impact values for wire G79 (overmatching) then expected for that wire although the actual values were accepted from the structural point of view. These impact values could be higher, if necessary, by increasing the content of CO2 % in the shielding gas.

Static Strength

The design provisions of EN 1993-1-8 (2002), which are identical to those proposed by CIDECT (1991) for the ultimate resistance, are used for predicting the joint capacity under axial load or bending loading. The results of the present study have demonstrated that the static strength equations in the above two specifications can be used for design purposes. For welded tubular X-joints under balanced loading conditions, those equations are

Axial loading

Chord failure:

$$N_{1,Rd} = \frac{k_p f_{y0} t_0^2}{\sin\theta_1} \frac{5,2}{(1-0.81\beta)} / \gamma_{M5} \qquad (1)$$

where kp is a coefficient that depends on the chord loading.

Punching shear failure $\left(d_1 \le d_0 - 2t_0\right)$:

$$N_{i,Rd} = \frac{f_{y0}}{\sqrt{3}} t_0 \pi d_i \frac{1+\sin\theta_1}{2\sin^2\theta_1} / \gamma_{M5} \quad (2)$$

In-plane bending

$$M_{ip,Rd} = 4{,}85 \frac{f_{y0} t_0^2 d_1}{\sin\theta_1} \sqrt{\gamma} \beta k_p / \gamma_{M5} \quad (3)$$

Punching shear failure $\left(d_1 \le d_0 - 2t_0\right)$:

$$M_{ip,Rd} = \frac{f_{y0} t_0 d_1^2}{\sqrt{3}} \frac{1+3\sin\theta_1}{4\sin^2\theta_1} / \gamma_{M5} \quad (4)$$

Out-of-plane bending

$$M_{op,Rd} = \frac{f_{y0} t_0^2 d_1}{\sin\theta_1} \frac{2{,}7}{1-0.81\beta} k_p / \gamma_{M5} \quad (5)$$

Punching shear failure $\left(d_1 \le d_0 - 2t_0\right)$:

$$M_{op,Rd} = \frac{f_{y0} t_0 d_1^2}{\sqrt{3}} \frac{3+\sin\theta_1}{4\sin^2\theta_1} / \gamma_{M5} \quad (6)$$

It should be noted that EN 1993-1-12 (2009) introduces a reduction factor equal to 0.8 for the steel grade under consideration. The experimental results from the present study indicate that – for over-matched welds in the range considered – the use of this reduction factor is not necessary.

Deformation capacity

The present results indicate that – for overmatched welds within the range considered in the present investigation – the increase the grade of the weld metal, results in a reduction of the deformation capacity of the tubular joints under monotonic loading conditions.

Fatigue Design

Existing design tools for welded tubular connections have been developed for ordinary steel grades up to 460 MPa, whereas tubular joints made of high-strength-steel are not covered by any international design code. Furthermore, EN 1993-1-9 (2002) provisions for welded tubular joints adopt the "classification of details" method, which is not applicable to the majority of tubular X-joints. Finally, the fatigue design of welded tubular connections in the low-cycle fatigue regime is an area not considered in current design practice. Therefore, the results from the present study constitute a significant contribution and can be used for the improvement of EN 1993 provisions for fatigue design.

In this perspective, the CIDECT (2001) guidelines can be used as a basis. They adopt the "hot spot" stress method, and they are applicable for a number of cycles greater than 103. The methodology consists of two main steps:

1. Stress Concentration Factors (SCF): The parametric SCF equations of CIDECT guidelines can be used for hot spot stress calculations in typical joint geometries. For more complex joint geometries, the corresponding SCF values can be computed through an appropriate finite element analysis, also described in the CIDECT guidelines.

2. Fatigue S-N Curve: The following fatigue S-N design curve proposed by the CIDECT guidelines can be used, which includes the effects of tube thickness. Using the hot spot stress (S) computed through an appropriate SCF value, this curve provides the fatigue design curve (N).

$$\log\left(N_f\right)=\frac{12.476-3\cdot\log\left(S_{rhs}\right)}{1-0.18\cdot\log\left(\frac{16}{t}\right)} \quad (7)$$

The extension of the above methodology into the low-cycle regime can be considered through an "equivalent elastic stress range" through a linear extension of the S-N curves in the log-log scale, connecting (a) the point of fatigue design strength predicted by equation (7), with (b) the point on the vertical axis corresponding to static strength (number of cycles equal to 1). Point (b) for static strength can be predicted by the relevant design equations, properly expressed in terms of the hot-spot stress. Using this approach, the corresponding design methodology results in safe predictions and could be adopted for design purposes in the low-cycle fatigue range. In addition, it can be adopted by EN 1993-1-9 towards a more rational fatigue design methodology for welded tubular connections, based on the hot spot stress.

D.7.2.2 Design guidelines and recommendations for bolted joints

This section firstly presents an overview on current methods available in literature for the design of bolted joints with circular flanges. Then, guidelines and recommendations are drawn from the current methods using the experimental and numerical results of the present project (Task 4.4 and Task 5.3).

D.7.2.2.1 Current methods for the design of flange bolted joints

Since about three decades, bolted joints with circular flanges have been investigated in many researches, e.g. [1, 2, 3, 7, 8 and 11]. Some models have been proposed and have been gradually improved through experimental, numerical and analytical investigations, leading to different guidelines for the design of such joints. The present section summarizes these models.

Definition of parameters

Geometric dimensions (Fig.7.2.1):

A: Cross-sectional area of a tube;

A_s: Throated area of a bolt;

d: Diameter of a bolt;

D: Outside diameter of a tube;

D_p: Diameter of bolt pitch circle;

D_f: Diameter of a flange;

a_w: Throat thickness of a weld;

e_1: Distance from the bolt axis to the outside surface of tube;

e_2: Distance from the bolt axis to the flange edge;

t: Tube thickness

$m = e_1 - 0,8\sqrt{2}a_w$;

$e' = \sqrt{D_f^2/4 - m^2} - D_p/2$.

Geometric coefficients:

$$k_1 = \ln\frac{D_p}{D-t};$$

$$k_2 = \frac{1}{2k_1}\left[2 + k_1 + \sqrt{k_1^2+4}\right];$$

$k_3 = \ln \dfrac{D_p / 2 + n}{D / 2 - t / 2}$ (n is the distance from the prying force to the bolt axis [1]).

Mechanic characteristics:

B_0: Total preload in all bolts of a joint;

B_u: Resistance of all bolts in a joint;

T: Applied tensile force;

$f_{u,f}$: Ultimate stress of flange;

m_u: Ultimate resistant moment of flange (per unit length);

ν: Poisson's ratio.

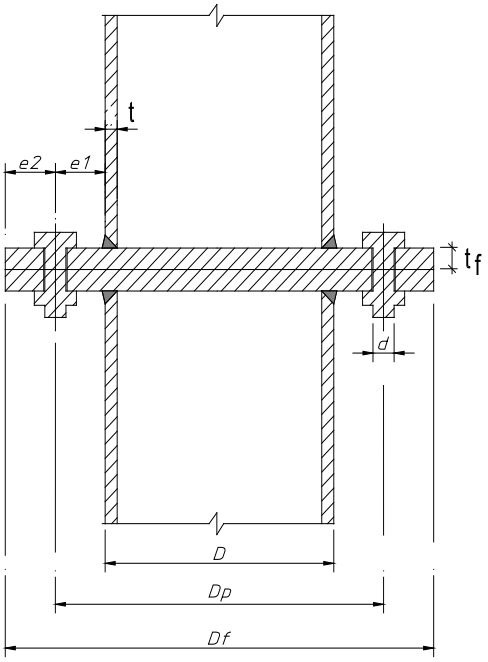

Fig.7.2.1. Geometric parameters for the considered joints

Remarks: As the objective is comparison between the methods and between the methods and the experimental results, all partial factors are taken to equal to 1.0 and they are not appeared in the formulas. Moreover, the yield strength and the plastic moment are replaced by the ultimate strength and the ultimate moment respectively.

Igarashi method [7]:

By applying limit analysis for the flanges, Igarashi proposed analytical formulas to determine the minimum required flange thickness and the minimum required number of bolts as follows:

$$t_f \geq \sqrt{\frac{2T}{f_{u,f}\pi k_2}};$$

$$B_u \geq T\left[1 - \frac{1}{k_2} + \frac{1}{k_2 \ln(D_f / D_p)}\right]. \quad (8)$$

With a joint where the geometrical and the material properties are defined, the capacity of the joint (T) can be obtain from above equations.

The Igarashi development has been used in CIDECT to propose guidelines for designing bolted joints with circular flanges [11].

Cao and Belle method [2, 3]:

Cao and Bell use a model assuming a linear elastic behaviour for the material; also, the prying forces and bolt forces are assumed to be uniformly distributed at the flange edges and at the bolt pitch circle respectively. With these assumptions, analytical formulations for the bolted joints were developed. Simplified formulas, tables and charts were also established for practical purpose. The main formulas are reported in here below.

Firstly, the bolt force is supposed to be in linear variation with the applied tension force according to two straight lines:

$$B = 1.1B_0 \quad (B \le 1.1B_0)$$
$$B = \mu T + 0.1B_0 \quad (B > 1.1B_0) \tag{9}$$

with μ, a parameter linking B and T which can be determined from the geometrical dimensions of the joints (the detail formulas to determine μ can be found in [2]).

Secondly, the bending moment in the flange at the weld toe and at the bolt pitch circle may be determined as follows:

$$M_{ri} = \frac{-T}{8\pi}\left[(1-\upsilon)\frac{D_f^2-(D-t)^2-(D_f^2-D_p^2)\mu}{D_f^2}+2(1+\upsilon)\left(\ln\frac{D_f}{D-t}-\mu\ln\frac{D_f}{D_p}\right)\right]$$
$$M_{rp} = \frac{T}{8\pi}\left[(1-\upsilon)\frac{D_f^2-D_p^2}{D_f^2}\left(\mu-\frac{(D-t)^2}{D_p^2}\right)+2(1+\upsilon)(\mu-1)\ln\frac{D_f}{D_p}\right] \tag{10}$$

With a joint for which the geometrical and material properties are defined, the ultimate capacity of the joint is limited by the force in the bolts and the bending moment in the flanges:

$$B \le B_u;$$
$$M_r \le M_u. \tag{11}$$

"Eurocode" concept [8]:

In fact, Eurocodes are not directly recommending guidelines for the design of bolted joints with circular flanges. However, using the concept of T-stub given in Eurocode 3, part 1.8 [4], CIDECT Research Project 5BP [8] extended this concept to such joints.

According to this concept, three failure modes are distinguished and formulas are proposed to predict the associated resistances for the joint:

Mode 1 resistance (thin flanges – full plastic mechanism in the flange):

$$T_1 = 2\pi m_p\left[1+\frac{D+D_p}{2m}\right], \tag{12}$$

Mode 2 resistance (intermediate flanges – yield lines in the flange + bolt failure):

$$T_2 = \frac{2\pi m_u + nB_u}{m+n}; \tag{13}$$

Mode 3 resistance (thick flanges – bolt failure):

$$T_3 = B_u. \qquad (14)$$

The failure mode of the considered joint is defined as the mode corresponding to the smallest resistance.

Couchaux method [1]:

Recently, Couchaux [1] has proposed a procedure combining Igarashi model for the plastic analysis aspect and the T-Stub concept. Five (5) failure modes are considered to estimate the joint resistance. Herein, only Modes 1, 2 and 3 are presented; Modes 4 and 5 are related to the resistance of the tubes and the welds, aspects which are not considered herein.

Mode 1 resistance (thin flanges):

$$T_1 = 2\pi m_u \left[1 + \frac{2}{k_1}\right], \qquad (15)$$

$$but \quad T_1 \le 2\pi m_u n_b \min\left(2; \quad 1 + \frac{2e}{\pi m}\right).$$

Mode 2 resistance (intermediate flanges):

$$T_2 = 2\pi m_u \left[1 + \frac{1}{k_3}\right] + B_u \left[1 - \frac{k_1}{k_3}\right]; \qquad (16)$$

Mode 3 resistance (thick flanges):

$$T_3 = B_u. \qquad (17)$$

Fatigue strength according to Eurocode 3 [5]

According to Eurocode 3, part 1.9 [5], the fatigue strength of joints may be calculated respecting the following steps:

- Define the critical zones where cracks have the possibility to develop; with a circular flange bolted joint, three critical zones may be identified as shown in Fig.7.2.2: on the tube at the weld toe, on the flange at the weld toe, and in the bolts.

- Assign to the critical zones the corresponding details as given in Eurocode 3, part 1.9 (Tables 8.1 - 8.10 and Table B1 of [5]).

- Then, calculate, for each detail, the reference stress ranges ($\Delta\sigma_C$) corresponding to a fatigue strength of two million cycles.

- Determine the stress ranges ($\Delta\sigma_R$), using the nominal stress range concept for the details belonging to Tables 8.1-8.10 of Reference [5] and the hot-sport stress range concept for the details belonging to Table B.1 of Reference [5].

- Compute the endurance (in cycles) of the details with a loading band with constant stress ranges:

$$N_{Ri} = 2x10^6 \left(\frac{\Delta\sigma_C}{\Delta\sigma_{Ri}}\right)^m \quad (m = 3 \quad for \quad N \le 5x10^6, \quad m = 5 \quad for \quad N > 5x10^6) \qquad (18)$$

- Finally, calculate the damage index of joints with the following formula:

$$D_d = \sum_i^n \frac{n_{Ei}}{N_{Ri}} \quad (19)$$

with n_{Ei}, the number of cycles associated to the stress range $\Delta\sigma_{Ri}$ for loading band I (for a constant loading i=1).

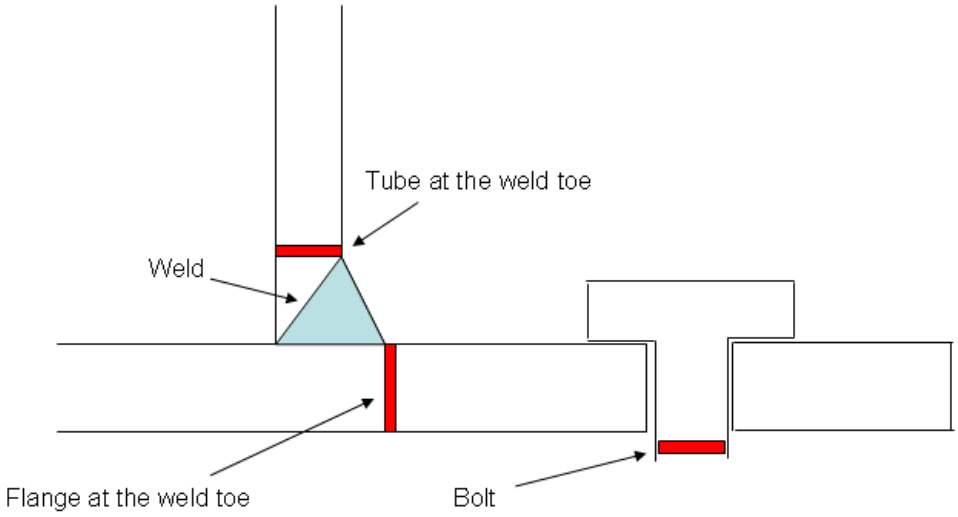

Fig.7.2.2. Critical zones in bolted joints (under fatigue loading)

Cyclic behaviour of bolted joints

The studies on the behaviour of bolted joints under repeated loadings are quite rare in the literature; some publications on the behaviour of T-stub under cyclic loading are available, e.g. [9, 10]. In the latter, methods to model the hysteretic loops of T-Stub under repeated loading are proposed. In [10] in particular, Piluso et al developed an analytical procedure to model the cyclic behaviour knowing the geometrical and material characteristics of T-Stub.

From the test results (Task 4.4), it can be observed that the hysteretic loops of bolted joints are similar to the ones of T-Stub. Therefore, as the development performed in case of monotonic loading [8], the T-Stub models could be extended to bolted joints in case of repeated loading.

D.7.2.2.2 Comparison with the experimental results

The details of the conducted experimental campaign and of the obtained results are presented in Deliverable D4.4 (corresponding to Task 4.4); also, numerical investigations conducted on the tested specimens are reported in Deliverable D5.3 (corresponding to Task 5.3).

In the following, the ultimate capacities and the failure modes of joints coming from the current methods are compared with the experimental results.

The geometrical and material properties of the two investigated joint configurations are summarized in Fig.7.2.3.

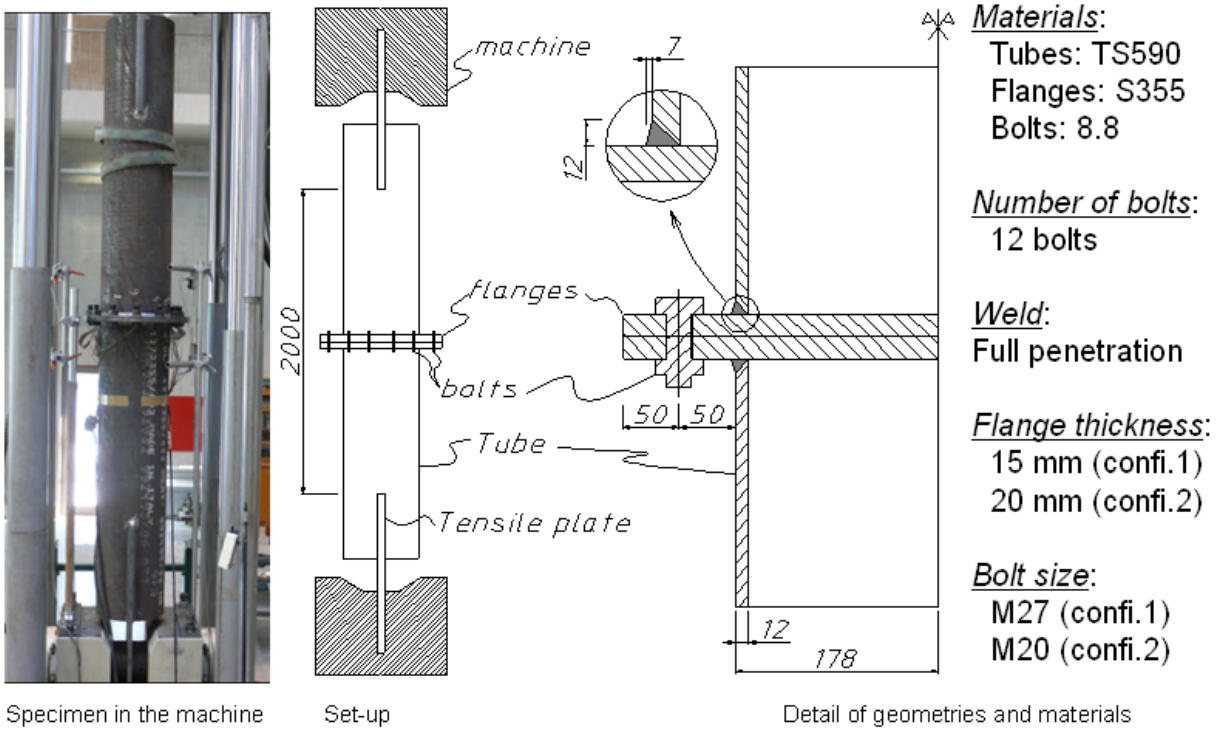

Fig.7.2.3. Description of the investigated joints

The summary of the results of coupon test performed on materials composing the tested specimens is reported in Table 7.2.1 (more details can be found in Deliverable D4.4).

Table 7.2.1: Results of coupon tests

Parameters	Plate 15mm	Plate 20mm	Tube	M27 bolts	M20 bolts
Yield strength (N/mm2)	387	384	822	857	850
Utimate strength (N/mm2)	544	529	881	930	930

With the above geometrical and material data and using the previously-described formulas, it was possible to estimate the ultimate resistances under monotonic loading and the fatigue strength of the investigated joints. The obtained results are summarized in Tables 7.2.2 and 7.2.3.

For calculating the fatigue strength of the tube, the constructional detail number 11 given in Table 8.5 of Reference [5] is used (see Table7.2.2). For this detail, the flange is made of a ring welded to the tube while the flange of the tested joints is made of a plate welded to the tube (i.e no hole is present in the flange); accordingly, the used detail is not fully corresponding to the actual configuration met in the tested joints. However, the used detail may be considered as the nearest detail; it is the reason explaining the selection of the latter.

The stress range on the tube is calculated as the nominal stress by dividing the axial force by the tube area.

Remark: no specific rules are given in Eurocode 3, part 1-12 [6] for the case of high strength steel.

Table 7.2.2: Used details in Eurocode 3, part 1.9 [5]

Detail category	Constructional detail	Description	Requirements
In Table 8.1 50	size effect for ⌀ > 30mm: $k_s=(30/⌀)^{0,25}$ 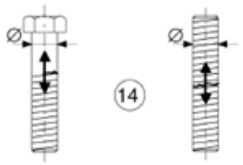	14) Bolts and rods with rolled or cut threads in tension. For large diameters (anchor bolts) the size effect has to be taken into account with k_s.	14) $\Delta\sigma$ to be calculated using the tensile stress area of the bolt. Bending and tension resulting from prying effects and bending stresses from other sources must be taken into account. For preloaded bolts, the reduction of the stress range may be taken into account.
In Table 8.5 71	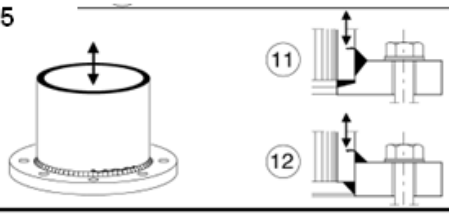	11) Tube socket joint with 80% full penetration butt welds.	11) Weld toe ground. $\Delta\sigma$ computed in tube.
40		12) Tube socket joint with fillet welds.	12) $\Delta\sigma$ computed in tube.
In Table B.1 100	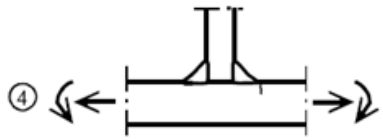	4) Non load-carrying fillet welds.	4) - Weld toe angle ≤60°. - See also NOTE 2.

Table 7.2.3: Comparison of the methods (static loading)

Method	Configuration 1		Configuration 2	
	Ultimate capacity (kN)	Critical components	Ultimate capacity (kN)	Critical components
Igarashi [7]	1466	flanges	1801	bolts
Bell and Cao [2,3]	1493	flanges	1596	bolts
“Eurocode” [8]	1944	flanges	2249	flanges + bolts
Couchaux [1]	1561	flanges	2161	flanges + bolts
Experimental	>2500	flanges + bolts	2320	bolts

Table 7.2.4: Comparison of the method (high cycle loading)

Method	Damage index	
	Configuration 1	Configuration 2
Eurocode (nominal stress) [5]	0.45	0.38
Eurocode (hot-spot stress) [5]	1.32	1.67
Experimental	1.00	1.00

D.7.2.2.3 Analysis of the comparisons

- The results coming from the current methods and the experimental tests are quite different, in both ultimate capacity and failure mode (Table 7.2.3). It can be observed that the ultimate capacity of the joints is always underestimated through the analytical models, what is on the safe side. However, as the

failure mode is not well predicted, it can lead to troubles in the design process; indeed, when the designer is looking for a ductile mode of failure (for instance, Modes 1 and 2 in the Eurocode and Couchaux concepts), the fact that the actual failure mode is not well predicted can lead to a lack of ductility.

- There are significant differences between Eurocode and test results concerning the fatigue strength of tube at the weld toe (Table 7.2.4). It is important to notice that the fatigue strengths given by Eurocode are not conservatives in comparison with test results. Even the geometries (ring/full flanges) and the material (normal/high-strength steel) are not corresponding between the used detail and the one of tested specimens, it cannot explain the observed differences. In fact, some inconsistency within the rules given in the Eurocode for this detail can be identified; indeed, the stress range in the tube at the weld toe is very sensitive to the geometries of the different components (tubes/flanges), what is not taken into account within the procedure of Eurocode 3, part 1.9 [5]. To improve the prediction given by the Eurocode, one solution would be to use the hot-spot stress (computed through FEM analyses or analytical approaches) in the concerned detail instead of the nominal stress as actually recommended in the Eurocode. In Task 5.3, detailed numerical simulations of the investigated joints were performed and validated through comparisons to the experimental results. Through these investigations, it was possible to extract the hot-spot stresses in the concerned detail (i.e. in the tube at the weld toe). Using these stresses, it leads to damage indexes as reported in Table 4 which are higher than the experimental ones, meaning that the prediction using the hot-spot stresses is conservative (i.e. on the safe side). Accordingly, through the investigations conducted within this project, one recommendation is to use the hot-spot stress instead of the nominal stress to determine the fatigue strength of this detail. As this aspect was only investigated for the two configurations studied within the present project, a perspective of the presented work would be to investigate if this conclusion remains valid for other joint configurations.

D.7.2.2.4 Conclusions

Combining the literature review and the experimental and numerical results of the present project (Task 4.4 (D4.4) and Task 5.3 (D5.3)), the following conclusions can be drawn for the design guidelines to be recommended for bolted joints with circular flanges.

Under monotonic loading:

The following methods have been considered herein: Igarashi method [7], Cao and Belle method [2, 3], Eurocode method [8] and Couchaux method [1]. On the estimation of the ultimate capacity of the considered joints, all above-mentioned methods are conservative; the observed differences between the method predictions and the experimental results are in a range of 4%-40%. The predictions given by the Eurocode method are the most accurate one.

Under fatigue loading:

(1) Through the preformed investigations, it has been demonstrated that the use of “detail number 11” of Table 8.5 in Eurocode 3, part 1-9 [5] (calculating the fatigue strength of the tube at the weld toe) leads to an overestimation of the fatigue strength, which is unconservative. Therefore, it is suggested to use the hot-spot stress concept for this detail. The latter can be estimated through finite element analyses (as performed in Task 5.3 – see D5.3) or through analytical methods using coefficients to take into account of the stress concentration [1]. With this method, it has been demonstrated that a conservative prediction of the fatigue strength can be obtained.

(2) The detail number 14 in Table 8.1 of Eurocode 3, part 1-9 [5] may be used to calculate the fatigue strength of the bolts, but the stress range in bolts should be estimated in two steps: (i) using finite element method to computer the stress in the bolts and (ii) applying the “Through thickness at the weld toe” method (see Deliverable 5.3) to calculate the structural stress that may be considered as the “nominal” stress, taking into account the bending and pre-stress effects as requested in Eurocode 3, part 1-9 [5].

(3) Detail category 100 as proposed in Eurocode 3, part 1-9 [5] can be applied to estimate the fatigue strength of the flanges at the weld toe. The “Through thickness at the weld toe” method (see Deliverable 5.3) or “Structural stress from the distance” method (i.e. Dong method, see Deliverable D5.3) should be adopted to capture the stress ranges from the stress given by finite element models.

(4) The initial deformation of the flanges due to the heat-affect during the weld procedure significantly influences to the stress range on the tubes and on the flange. Therefore, the initial deformation should be taken into account in the finite element modelling if an economic design is needed.

Under repeated loading (low cycle fatigue)

For bolted joints with circular flanges, it is suggested to extend the model of Piluso [10] initially developed for the modelling of T-stub.

D.7.2.3 Behavior of HSS CHS members under extreme cyclic loading conditions

The behavior of tubular members under extreme cyclic loading conditions, with emphasis on bending, has several particularities that should be recognized by the design engineers. Nevertheless, modeling of those particularities is a demanding topic that requires high-performance computations with advanced numerical tools.

The main characteristic of the structural behavior of tubular members under strong cyclic loading, associated with significant inelastic deformations of alternative sign, is the accumulation of plastic deformation. More specifically, the response of a steel tube under monotonic loading defines the maximum bending moment of the tube, and the corresponding deformation capacity. If one considers cyclic bending of the tube in the inelastic range, but within the load and deformation limits defined for monotonic conditions, the tube might not be safe. Under this repeated loading, accumulation of deformation occurs, resulting in excessive strains and eventually in the formation of local buckling of the tube wall or – in a few cases – fracture of the tube near the two ends.

The above phenomenon can be regarded as the interaction of the effects from two sources:

- At the material level, experiments in steel specimens have indicated that under uniaxial stress-controlled loading conditions in the plastic range about a non-zero mean stress the material exhibits “ratcheting” or “cyclic creep”, where cycle-by-cycle the hysteresis loops translate in the direction of maximum stress, resulting in an increase of the maximum strain. In addition, in the case of strain-controlled loading conditions, while a constant stress is applied on the specimen in a normal direction, a cumulative increase of the strain amplitude in the direction of the applied stress results, a phenomenon referred to as “biaxial ratcheting”. Those phenomena have been well-documented experimentally for several steel materials and several attempts have been made to develop numerical models that describe them in an accurate manner [12, 13].
- At the structural level of the bent tube, it has been widely recognized that the bent tubes exhibit cross-sectional ovalization prior to a maximum moment is reached and well before local buckling occurs. This ovalization reduces the plastic moment and enables the formation of local buckling. Furthermore, it induces hoop stresses and strains in the tube, so that the state of stress and strain in the critical zone of the bent tube is biaxial, referring to the above “cyclic creep” phenomenon.

To investigate the above structural behavior, it is important for the designer to identify whether the tubular member is subjected to load-controlled or deformation-controlled action. Experimental data and numerical results have shown that in both cases, the accumulation of deformation in the tubular member may result in failure in the form of bucking or fracture. Nevertheless, it has been recognized that cyclic load-controlled conditions about a non-zero mean load value is the most dangerous case, where maximum curvature may increase rapidly resulting in significant strain amplification and member failure, together with an progressive increase of cross-sectional ovalization [14]. A typical result from numerical simulation of cyclic bending of a ∅323.9/10 high-strength CHS member, is shown in Figure 7.2.4.

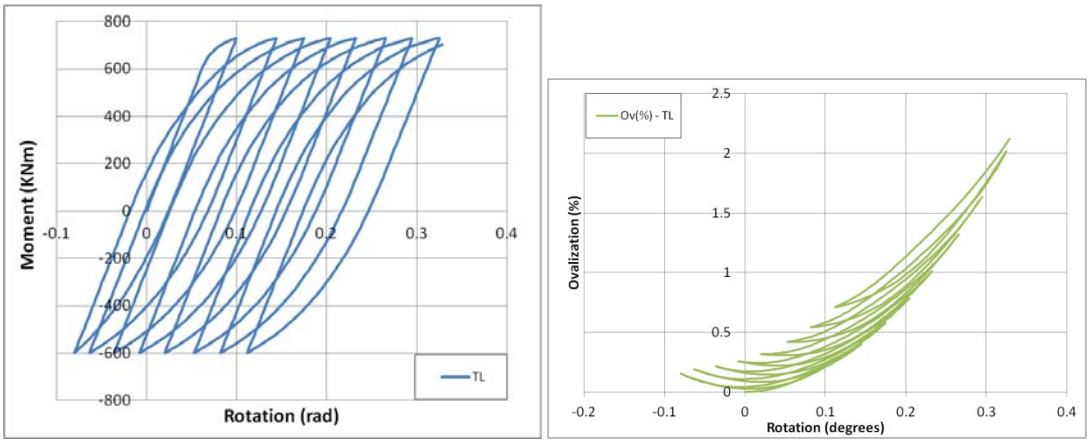

Fig 7.2.4: Structural response of a ∅323.9/10 high-strength CHS member, under non-symmetric moment-controlled cyclic loading.

Modeling of the above behavior may not be a trivial issue. It is required that the engineer performs a nonlinear analysis, which couples:

- Geometric nonlinearity, in the sense that the numerical model should be able to represent the change of geometry and the flattening of the cross-section [14]
- Material nonlinearity, through the use of advanced numerical models. Cyclic plasticity related phenomena such as the Bauschinger effect and ratcheting [12, 13].

Concerning the material model to be adopted, a simple yet effective model is a J2 flow model with mixed (isotropic and kinematic) hardening. This model is able to predict the abrupt change of the material stress-strain curve when initial yielding occurs, as well as the smooth transition into the plastic range upon load reversal due to Bauschinger effect. Another suitable plasticity model for such applications is the Chaboche model [15]. If this model is adopted, caution should be paid to the increased plastic deformations predicted at the initial loading phase. The two aforementioned models are available in many commercial finite element codes. Finally, other more advanced plasticity models, such as those adopting the "bounding surface" concept (e.g. Dafalias – Popov, Tseng-Lee), that are able to capture the cyclic plasticity phenomena discussed previously are suggested (if available) for this type of simulations. The expected simulation accuracy by this class of models is increased compared to the more simple models.

An important issue towards successful modeling concerns the calibration of the above plasticity models, with respect to appropriately chosen experimental data. Many steel materials exhibit a change (increase or decrease) of the elastic stress range (size of the yield surface) after consecutive loading in the plastic regime. For accurate numerical predictions, it is necessary to define the maximum change of the size of the yield surface and the rate that this takes place with respect to the applied plastic deformations. In addition, the ratcheting rate under stress-controlled plastic cyclic loading should be also predicted accurately. In order to calibrate the adopted plasticity model to predict accurately the aforementioned phenomena, two types of material tests should be conducted:

- Strain-controlled cyclic loading tests at various strain ranges, near the stress-range expected, in order to examine the change of the yield surface size and its rate.
- Stress-controlled cyclic loading tests at various mean stress levels, in order to examine the mean stress effect on the ratcheting rate.

The material parameters of the adopted plasticity model should be calibrated accordingly. For the Chaboche model, a calibration method is described in [16].

D.7.2.4 Buckling resistance of HSS CHS columns in bending and axial compression

Members under axial compression plus bending develop specific load-carrying behaviour in the different ranges of slenderness. Depending on the emphasis given to the different ranges, different concepts of interaction formulae have been proposed in the past. The present approach of EN1993-1-1 [17] is based on the linear-additive form of interaction formula derived from linear-elastic buckling

response, where the effect of the axial force and the bending moments are linearly summed and the nonlinear effects are accounted for by specific interaction factors. Latest version of the Eurocode 3 has incorporated some new design formulae that enable a more economic design. This is particularly the case for the rules for the verification of members subjected to combined bending and compression. Moreover Part 1-12 of Eurocode 3 [6] has been recently published that extends its scope to strength grades up to S700. Part 1-12 gives a few changes and some additional rules to the already existing parts of Eurocode 3 in order to make them applicable to steel grades up to S700.

In the frame of this project an HSS CHS is studied which nominal dimensions are 193.7mm in diameter and 10mm in thickness. Material is seamless quenched and tempered tube of nominal strength class S590. Considering actual mechanical properties of columns (f_y = 694 MPa; D/t = 19.4) the cross section is classified as Class 2 in accordance with EN 1993-1-1 while considering nominal strength (f_y = 590 MPa) a Class 1 is concerned.

Full-scale tests have been performed at two different column lengths

- Short (member slenderness 28.4) relevant for cross sectional behaviour
- Long (member slenderness 74.6) relevant for member behaviour

The outcome of experimental data (task 3.3) are compared with Eurocode 3 predictions in the following N-M interaction diagrams (Figure 7.2.5). The EC3 predictions are calculated following both methods presently reported in the standard, namely Method 1 (m1) and Method 2 (m2) [18], for the scope of comparison safety coefficients are set to 1.00. The experimental results are on the boundary safe side of the interaction diagrams indicating that recommended formulae are consistently extended to HSS members for the slenderness range investigated.

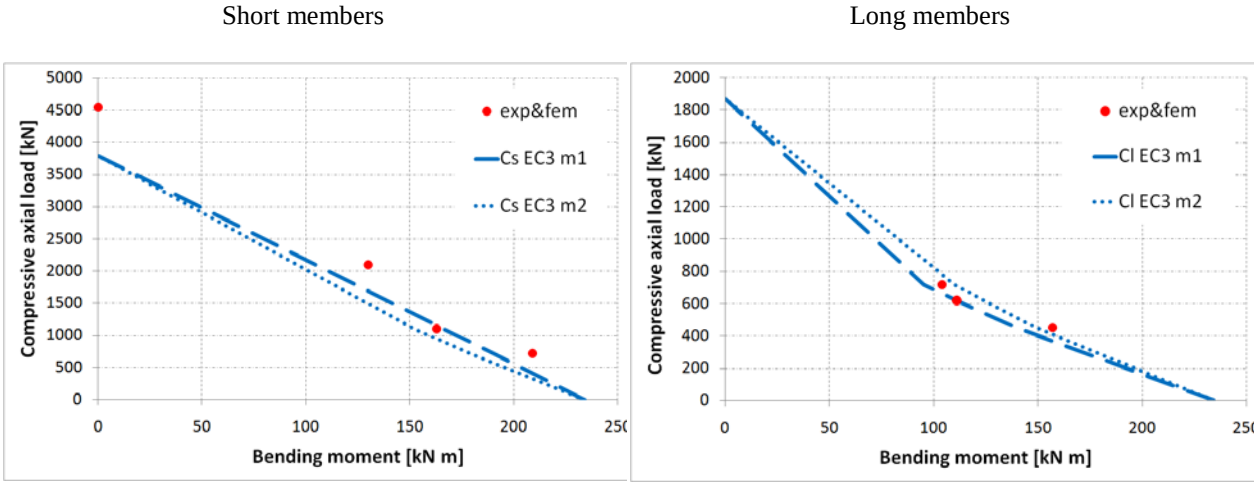

Figure 7.2.5. HSS CHS interaction M-N diagram: comparison between Eurocode 3 design recommendations and experimental results.

Experimental data and finite element analysis outcomes are in this section presented in a form to make it consistent with Eurocode 3 interaction formulae. In particular second order moment imposed by extensions of the testing machine are explicitly reported as follow.

Full scale testing rig is such that the column is connected to the machine hinges via rigid extensions named “codolo” able to transmit rigid motion to the column ends (Figure 7.2.6). In the case of combined load test where constant axial compressive load is applied, once the specimen starts to rotate a second order moment induced by “codolos” is applied at the column ends.

Figure 7.2.6. Full scale testing arrangement

Experiment outcome report applied loads at the machine hinges hence moments induced by “codolos” are not explicitly quantified. This is an inconvenience when comparing experimental data with design interaction formulae that refers to the column loaded at its ends, as in the case of Eurocode 3.

Stating that “codolos” are much stiffer than column, knowing the rotation at the hinges, it is possible to explicitly show the second order moment induced by “codolos”. The experimental curves modified with explicit contribution of “codolos” are reported In Figure 7.2.7b and Figure 7.2.8b for short and long members respectively, those were used for comparison with Eurocode 3 interaction formulae (Figure 7.2.5).

(a)

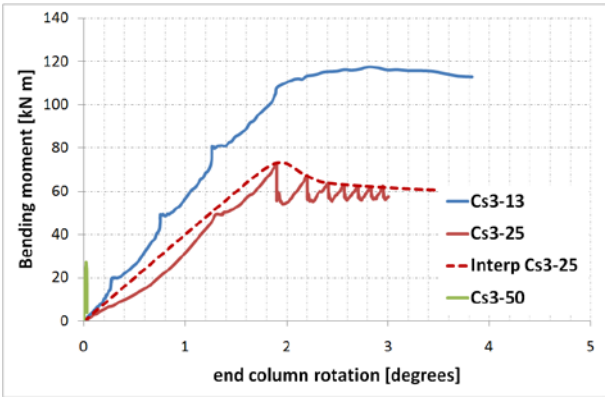

(b)

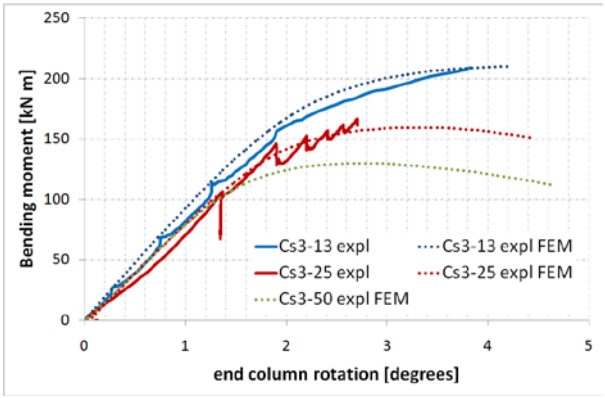

Figure 7.2.7 Short column combined load tests: moment vs. rotation original corves (a); modified curves with explicit contribution of “codolos”(b).

(a)

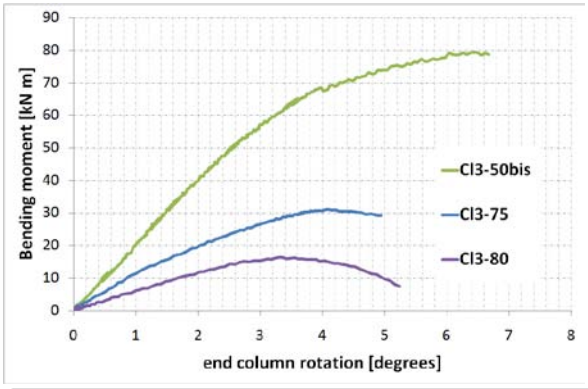

(b)

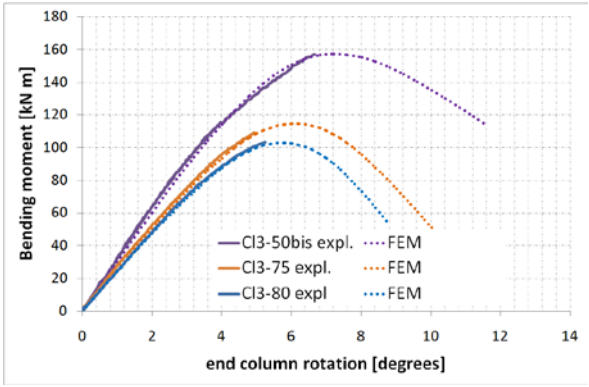

Figure 7.2.8. Long column combined load tests: moment vs. rotation original corves (a); modified curves with explicit contribution of “codolos”(b).

D.7.2.5 References

[1] Couchaux M. Comportement des assemblages par brides circulaires boulonnés. PhD thesis 2010, INSA of Rennes, France.

[2] Cao J.J. & Bell A. J. Determination of bolt forces in a circular flange joint under tension force. Int. J. Press. & Piping 68 (1996) 63-71.

[3] Cao J.J. & Bell A. J. Design of Tension Circular Flange Joints in Tubular Structures. Engineering Journal/First Quarter (1997) 17-25.

[4] Eurocode 3: Design of steel structures - Part 1-8: Design of joints. EN-2005.

[5] Eurocode 3: Design of steel structures - Part 1-9: Fatigue. EN-2005.

[6] Eurocode 3: Design of steel structures - Part 1-12: Additional rules for the extension of EN 1993 up to steel grades S700. CEN-2007.

[7] Igarashi S. et al. Limit design of high strength bolted tube flange joint, Part 1 and 2. Journal of Structural and construction engineering transactions of AIJ, Department of Architecture reports, Osaka University, Japan, August 1985.

[8] Jaspart J.P. et al. Development of a full consistent design approach for bolted and welded joints in building frames and trusses between steel members made of hollow and/or open sections: application of the component method. Volume 1: practical guidelines. CIDECT research project 5BP (2005).

[9] Nemati N. et al. Numerical modelling of cyclic behaviour of the basic components of steel end plate connections. Advances in Engineering Software 31(2000) 837-849.

[10] Piluso V, Rizzano G. Experimental analysis and modelling of bolted T-stub under cyclic loads. Journal of Constructional Steel Research 64(2008) 655-669.

[11] Wardenier J. et al. Design guide for circular hollow section (CHS) under predominantly static loading. CIDECT 2008.

[12] Hassan, T., and Kyriakides, S., (1992). “Ratcheting in cyclic plasticity, Part I:Uniaxial behavior”, Int. Journal of Plasticity, vol. 8, pp.91-116.

[13] Hassan, T., Corona, E., and Kyriakides, S., (1992), “Ratcheting in cyclic plasticity, Part II: Multiaxial behavior”, Int. Journal of Plasticity, vol. 8, pp.117-146.

[14] Shaw, P.K., and Kyriakides, S., (1985) “Inelastic analysis of thin-walled tubes under cyclic bending”, Int. Journal of Solids and Structures, vol. 21, pp.1073-1100.

[15] Chaboche, J.L., (1986). “Time-independed constitutive theories for cyclic plasticity”. Int. Journal of Plasticity, vol. 2, pp. 149-188.

[16] Lemaitre, J., and Chaboche, J.L.,(1990), Mechanics of solid materials. Cambridge University Press.

[17] EN1993-1-1:2005. Design of steel structures. Part 1-1: General rules and rules for buildings

[18] ECCS Publication No. 119. Rules for Member Stability in EN 1993-1-1: Background documentation and design guidelines. 2006.

D.7.3. Report on maintenance and durability of HSS tubular structures

Structural aging may cause the integrity of structures to evolve over time (e.g., a hostile service environment may cause structural strength and stiffness to degrade). Any evaluation of the reliability or safety margin of a structure during its service life must take into account the uncertainties. Time-dependent reliability analysis methods provide the framework for dealing with uncertainties in performing condition assessment of existing and aging structures, and for determining whether in-service inspection and maintenance is required to maintain their performance at the desired level [1]. Bayesian updating techniques are very useful when faced with two sets of uncertain information and a planner needs to know which to believe. Bayesian updating uses both the prior information and new inspection information to account for the relative uncertainty associated with each [2].

Several studies in the past have shown that the reliability of the bridge decks depends significantly on the rate of corrosion of the steel [2] [3] [4]. The safety of the system as a whole can be defined by the safety of each component, deck, girders, piers, etc, and how each component interacts within the system. The safety of the deck components, such as tubular truss sections and connections of the footbridge Ponte del Mare of Pescara, are the focus of this investigation, see Figure 7.3.1.

Figure 7.3.1 section of the deck of the footbridge with CHS trusses.

D.7.3. 1 Limit states for the reliability of the footbridge

The performance or reliability of a structural system can be evaluated based on different limit states, most notably safety and serviceability limits. Both the safety and serviceability can play a significant role in determining the reliability of a structure; this investigation considers both limit states.

Ultimate/Safety Limit State

Safety margin, $SM = R - S \geq 0$

where R= capacity or strength, S= demand or stress.

Serviceability Limit State

Deflection, $\delta \leq L/500$

Deck Rotation, $\theta \leq 5.48\% \rightarrow$ corresponding to 21 cm of lateral deck deflection

D.7.3. 2 General corrosion model

The resistance of the structure changes due to the reduction of cross-sectional area of tubular steel trusses under corrosion assumed at the outer surface. At any time t, the reduced section area A(t) of a tube truss is given by the following Equation

$$A(t) = \frac{\pi}{4} \cdot \left[[D_0 - 2 \cdot r_{corr} \cdot W \cdot N \cdot (t - T_{corr})]^2 - {D_i}^2 \right] \quad (1)$$

where A(t)= area of a truss at time t (mm^2), t= time (years), D_o and D_i = outer and inner diameter of tube under corrosion (mm), T_{corr}= corrosion initiation time (years) – 10 years, r_{corr}=corrosion rate (mm/year) – 0.058 mm/year -, W= a weight coefficient taking into account the global positioning of the trusses w.r.t the sea canal; and N is a random number between 0 and 1 to consider the spreading of corrosion along each member – 0 implies no corrosion; 1 implies complete corrosion along a member -.

Corrosion rate: r_{corr}

The corrosion rate of HSS steel in an environment near the sea (at 1% NaCl from KIMAB tests in WP3) is considered as Gaussian distributed with mean value $\mu = 0.058$ mm/year and standard deviation $\sigma = 0.01224$ mm/year. The general formula of a Gaussian probability density function is showed in Eq(2):

$$F(x) = \frac{1}{\sigma \cdot \sqrt{2\pi}} \cdot e^{-\frac{(x-\mu)^2}{2\sigma^2}} \quad (2)$$

The distribution of the resulting corrosion rate r_{corr} of the footbridge is presented in Figure 7.3.2a.

Corrosion initiation time: T_{corr}

The distribution of corrosion initiation time is used to determine when corrosion will begin at the trusses surfaces. It has been considered a lognormal (Type1) probability distribution showed in Eq(3) with a mean value $\mu = 10$ years and standard deviation $\sigma = 1.5$ year because an initial painting guarantees for 10 years of corrosion resistence.

$$F(x) = \frac{1}{\sqrt{2\pi \cdot x \cdot \sigma}} \cdot \exp\left(-\frac{1}{2} \cdot \left(\frac{\ln x - \xi}{\delta}\right)^2\right) \quad (3)$$

With $\delta = \sqrt{\ln\left[\left(\frac{\sigma}{\mu}\right)^2 + 1\right]}$ and $\xi = \ln \mu - 0.5 \cdot \delta$

The distribution of the resulting corrosion initiation time Tcorr of the footbridge is presented in Figure 7.3.2b.

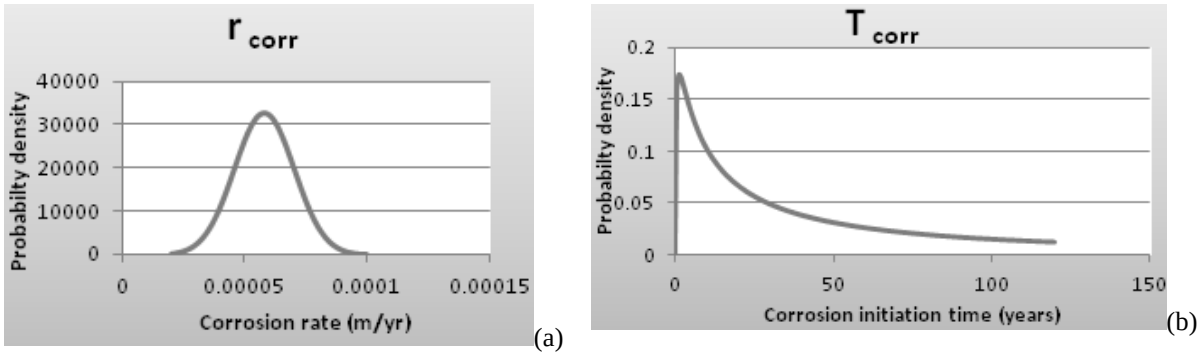

Figure 7.3.2 Probability density function of a) corrosion rate and, b) corrosion initiation time

Local effect of corrosion: N

To take into account the distribution of the corrosion along the truss, it has been defined one parameter N that is a value between 0 (no corrosion) to 1(complete corrosion). It has a uniform distribution according to Eq(4).

$$F(x) = \begin{cases} \frac{1}{b-a} & \text{for } x \in [a, b] \\ 0 & \text{otherwise} \end{cases} \quad (4)$$

Global effect of corrosion: W

W is a weight factor. The trusses located over the sea canal have higher probability of corrosion (W=1) than the one positioned at the ends of the footbridge (W=0.7). This global effect of corrosion is assumed to be linear with the distance from the sea canal (Eq(5)).

Considering the x value as the general point along the deck, the value of W starts from 1 over the sea (10 meters) and ends at the farthest point as 0.7 (at x=65 m and x = - 65 m).

$$W = \begin{cases} 0.004 \cdot x + 0.96 & x \in \{-65m; 10m\} \\ -0.005455 \cdot x + 1.054545 & x \in \{10m; 65m\} \end{cases} \quad (5)$$

Figure 7.3.3 provides the trend of W parameter.

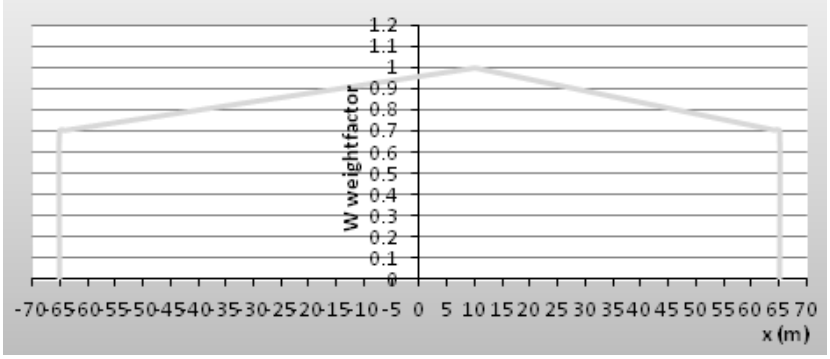

Figure 7.3.3 Global effect of corrosion along the footbridge

Yield strength of steel: F_{ys}

A Gaussian distribution is considered for the yield strength of the HSS steel. Its mean value is μ =640 MPa and the standard deviation is σ =16.67 MPa (based on the test data of the project). PDF is shown in Figure 7.3.4.

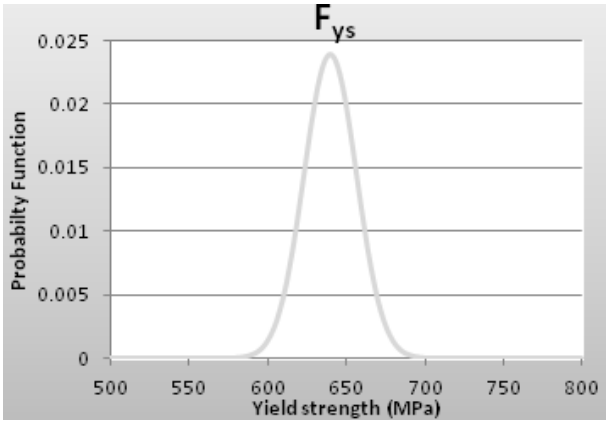

Figure 7.3.4 PDF of the yield strength of HSS steel

Wind load

The reliability model incorporates a time-dependent evaluation of the load effects on the deck. The maximum live load is assumed to increase over time since the likelihood of extreme loading conditions increases over time. For the wind load was chosen a Weibull probability density function. This choice distribution is according to [5]. For the ultimate limit state (return period 50 years) the wind speed, from sea to earth is 33.5 m/s and from earth to sea is 27 m/s. These two values come from the CNR DT207-2008 [6].

The corrosion model is implemented with the worst value that is 33.5 m/s. Eq(6) shows the Weibull PDF:

$$F(x) = 1 - e^{-\left(\frac{x}{\lambda}\right)^k} \quad (6)$$

where k is the exponent of the Weibull distribution and λ is the scale factor.

The annual values of the two parameters k and λ were calculated according to [7]. All the formulation is based on the definition of the characteristic value: it's the value that has the 95% of the probability to occur. So the values of the two parameters of the Weibull distribution are shown in Table 7.3.1 and plotted in Figure 7.3.5.

Table 7.3.1 Values of Weibull distribution parameters for the wind and pedestrian load

	Wind Load		Pedestrian Load	
Years	k	λ	k	λ
5	8.050180849	25.76829918	17.2093990	3.49671724
10	10.37928142	27.59401980	22.19242045	3.614507338
15	11.7952008	28.5362082	25.20095759	3.673781184
20	12.815558	29.1594489	27.36185466	3.712442626
25	13.6136983	29.6202114	29.04883164	3.740751544
30	14.2692432	29.9833163	30.43239207	3.76289963
35	14.8254537	30.281606	31.60505556	3.780989727
40	15.3084739	30.5339203	32.62239641	3.796218943
45	15.7353185	30.7520258	33.52087037	3.809330286
50	16.1176835	30.9437423		

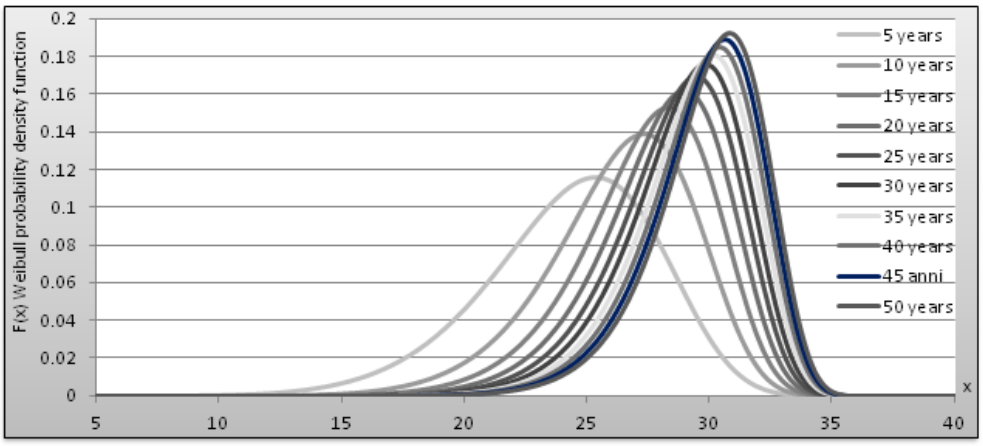

Figure 7.3.5 PDF of wind load considering different years

Pedestrian load

It is a load constituted from the compact crowd with intensity of 4 KN/m^2. As said before, the maximum live load is assumed to increase over time since the likelihood of extreme loading conditions increases over time. In other words, as more traffic crosses the bridge over time, the probability that the bridge will have experienced an extreme load increases. For this live load of pedestrian was chosen a Weibull probability density function (Eq(7)).

The annual values of the two Weibull parameters were calculated from the information of the characteristic value of pedestrian load: 4 KN/m^2 in 50 years for 95% confidence level. The results are shown in Table 7.3.1 and plotted in Figure 7.3.6.

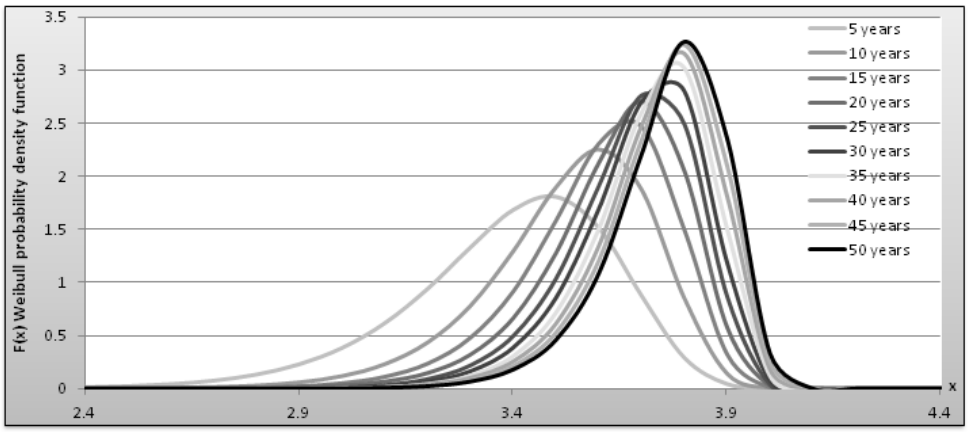

Figure 7.3.6 PDF of pedestrian load considering different years

D.7.3. 3 Simulations in ANSYS and main results

Simulations were performed for 5 to 50 years on the numerical model in ANSYS using Monte Carlo Simulation (MCS) technique and Latin hypercube sampling to accelerate convergence. Two hundred (200) iterations were run for each analysis. Two types of loading conditions were considered, i.e. with the wind and without the wind.

D.7.3. 3.1 Results of the parameters considering wind load

Maximum displacement

Figure 7.3.7 illustrates the time variation of the maximum displacement of the footbridge deck with wind load. It increases from the mean value of 0.251375 m at 5 years to the mean value of 0.2682 m at 50 years. The standard deviation remains almost constant over time.

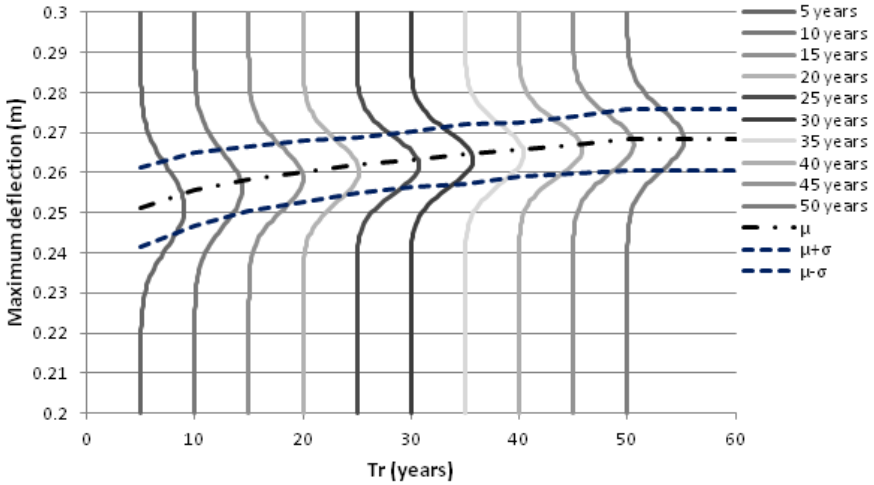

Figure 7.3.7 Maximum deck deflection

Maximum rotation

The maximum rotation of the deck is shown in Figure 7.3.8 where is easy to see the rapid increase of he mean value. It starts from 4.812 % at 5 years and goes to 5.409 % at 50 years. Also the standard deviation increases over time due to increasing of uncertainties from the value of 0.0016679 to 0.00236.

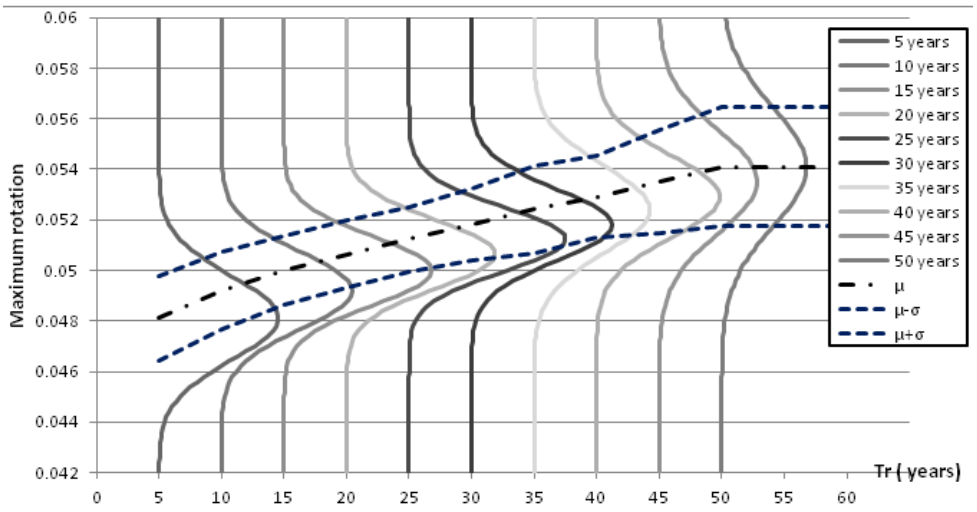

Figure 7.3.8 Time variation of maximum rotation of the cycling deck of the bridge considering wind load

Safety Margin

The safety margin is the difference between the resistance (strength) and the load effect (stress) of the deck. A positive safety margin indicates that the resistance is greater than the load effect and therefore the deck is safe. Conversely, a negative safety margin indicates that the deck is unsafe.

Figure 7.3.9 illustrates the change in the predicted safety margin distributions over time for a 50 year time horizon. The mean value of the safety margin distribution drops from 257.78 MPa initially to 243.62 MPa at 50 years. The standard deviation of the safety margin distribution increases slightly over time due to increasing uncertainties.

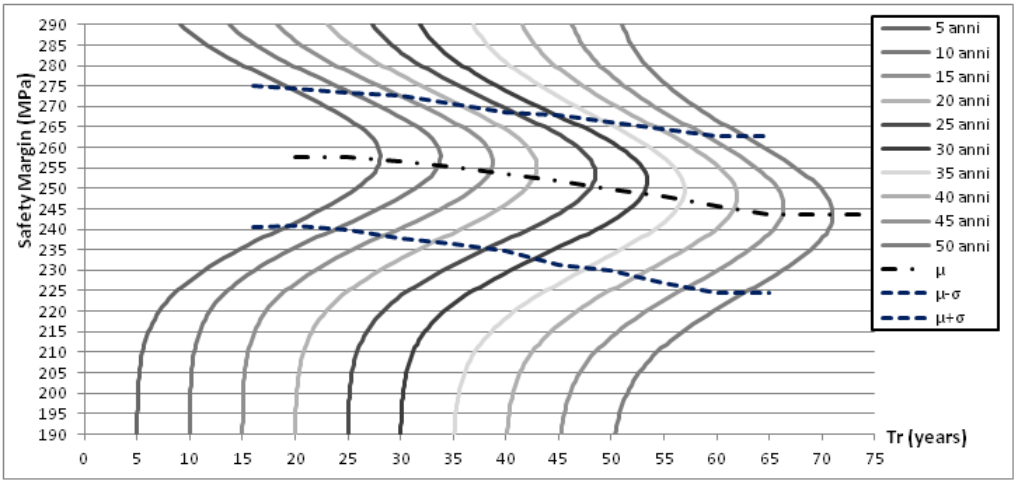

Figure 7.3.9 Safety margin (MPa) of the footbridge deck

D.7.3. 3.2 Results of the parameters without considering wind load

Maximum displacement

Figure 7.3.10 illustrates the time variation of the maximum displacement of the footbridge deck without wind load. It increases rapidly from the mean value of 0.2599 m at 5 years to the mean value of 0.28175 m at 50 years. The standard deviation decreases over the time from 0.009787 m to 0.007288 m.

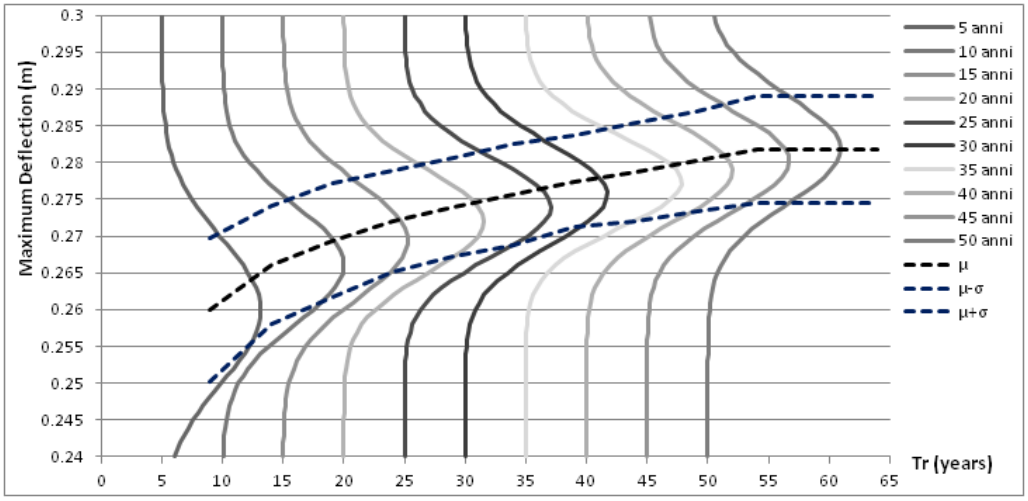

Figure 7.3.10 Time variation of maximum displacement of the footbridge deck without wind load

Maximum rotation

The maximum rotation of the deck is shown in Figure 7.3.11. It is increasing from 4.916 % at 5 years and goes to 5.5902 % at 5 years. Also the standard deviation increases over time due to increasing of uncertainties from the value of 0.001652 to 0.002348.

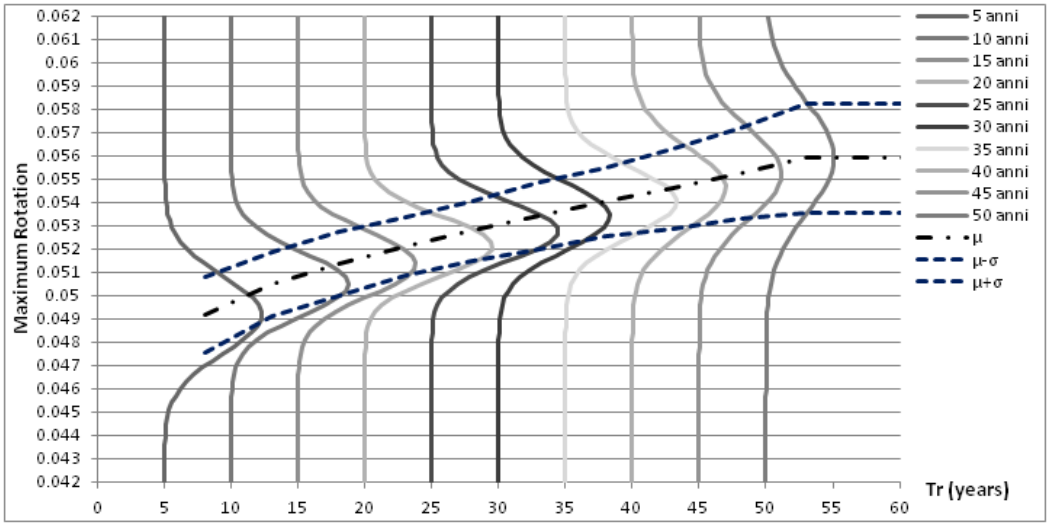

Figure 7.3.11 Maximum rotation of the footbridge deck

Safety Margin

Figure 7.3.12 illustrates the change of safety margin distributions over time for the 50 year time horizon. The mean value of the safety margin distribution drops from 254 MPa initially to 236.66 MPa at 50 years. The standard deviation of the safety margin distribution increases slightly over time due to increasing uncertainties from 16.747 MPa to 20.628 MPa.

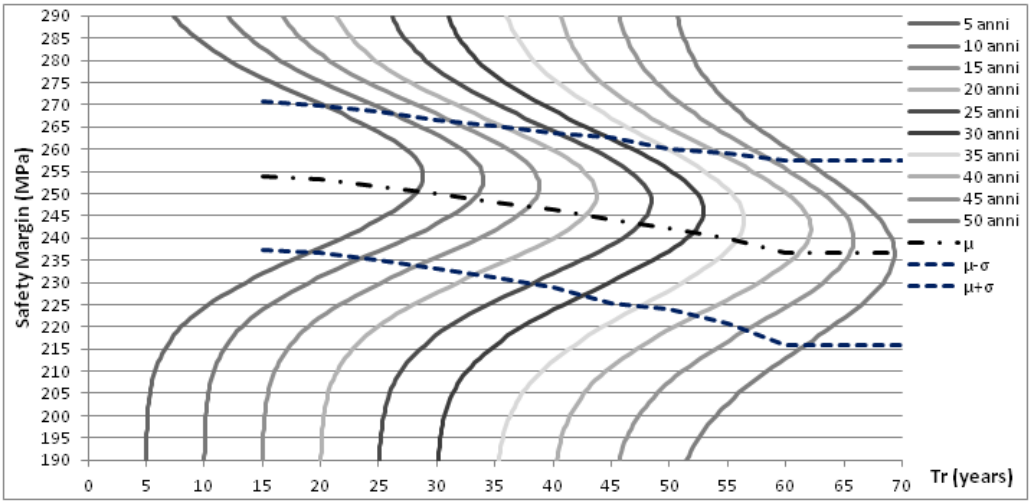

Figure 7.3.12 Safety margin of the footbridge deck

D.7.3. 4 Reliability index and probability of failure

A convenient method for describing the safety of a structural component or system is with the reliability index β, or the probability of failure P_f. According to the Annex C of the Eurocode '0' [8], the β and the P_f are related as:

$$P_f = \Phi(-\beta) \tag{7}$$

where Φ is the cumulative distribution function of the standard normal distribution.

The limit states of the maximum deflection- that should be less than L/500, and the limit state of the safety margin- that should be greater than 0, are satisfied. However, the calculations and the graphs showed that the maximum rotation doesn't satisfy the limiting rotation value of 5.48%. Therefore, we shall calculate the time dependent reliability evolution for the maximum rotation limit state.

The P_f and β are plotted with time for the rotation limit state in Figure 7.3.13 and Figure 7.3.14, respectively for the live load with and without considering the wind. In Figure 7.3.14, the limiting value of β is drawn from the Annex C of the Eurocode '0' [8] that means that β should be greater than 1.5 at 50 years.

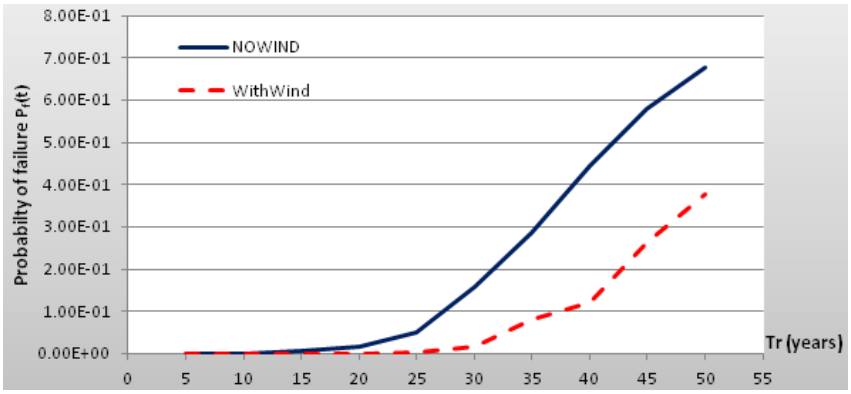

Figure 7.3.13 Time variation of probability of failure of the footbridge

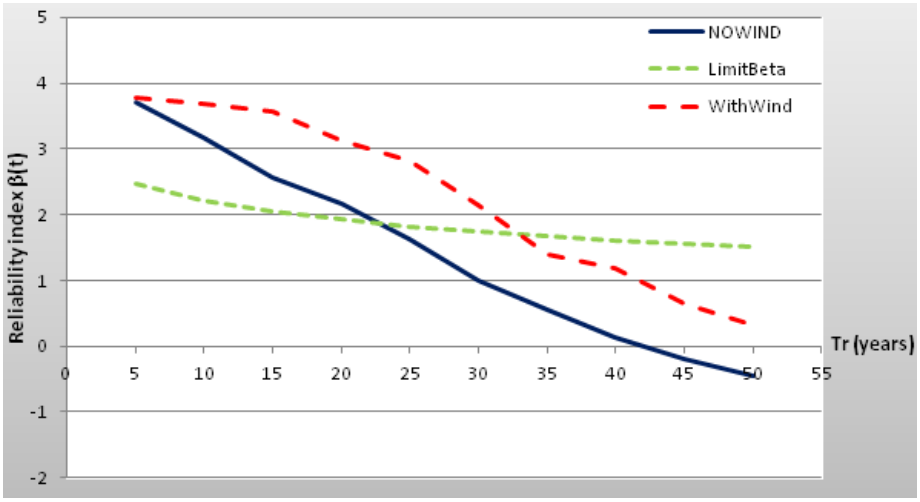

Figure 7.3.14 Time variation of reliability index of the footbridge deck

The value of β crosses the limiting value at about 23 years and 33 years for the case without and with wind. This shows that wind acts to increase the reliability of the footbridge structure owing to lifting effects. Moreover, the decision should be based on the critical case i.e. without wind. Therefore, the repair and/or retrofit plan should be activated before 23 years of the life of the footbridge to increase its reliability index. Bayesian estimation

Bayesian updating techniques are very useful when faced with two sets of uncertain information and a planner needs to know which to believe. Bayesian updating uses both the prior information and new inspection information to account for the relative uncertainty associated with each.

Assume that prior to an inspection, a random variable Θ was believed to have a density function $f'(\Theta)$ where Θ is the parameter of that distribution (i.e., the deterioration model). During an inspection, a set of values $x_1, x_2, ..., x_n$ representing a random sample from a population X with underlying density function f(x) are observed and are fit to a new density function $f(x_i)$ (i.e., the visual inspection results). The updated or posterior density function $f''(\Theta)$ which uses both sets of information and provides the best use of both can be expressed as [2]

$$f''(\Theta) = kL(\Theta) f'(\Theta) \tag{8}$$

where L(Θ)= likelihood function; and k= normalizing constant. For the case where both $f'(\Theta)$ and f(x) are normally distributed, the posterior function $f''(\Theta)$ is also normally distributed and has the mean value and standard deviation, respectively, as

$$\mu'' = \frac{\mu(\sigma')^2 + \mu'(\sigma)^2}{(\sigma')^2 + (\sigma)^2}, \sigma'' = \sqrt{\frac{(\sigma')^2(\sigma)^2}{(\sigma')^2 + (\sigma)^2}} \tag{9}$$

where μ, μ', and μ'' = mean values of the inspe ction results, the prior distribution, and the posterior distribution, respectively, and σ, σ', and σ'' = standard deviations of those same distributions.

We used the distribution of input parameters r_{corr}, T_{corr}, N, W, U and A_0. Moreover, if the new data are arrived, the posterior distributions of these inputs will change according to Eq (8). Footbridge of 'Ponte del Mare' is newly constructed. Therefore, we don't have the data for Bayesian update. However, by measurement data of wind speed, pedestrian load, distribution of corrosion locally and globally, PDF distributions could be updated. The new distribution values could be used in the model that will give a modified reliability of the footbridge

D.7.3. 5 General procedures for the inspection and maintenance of a footbridge

It is recommended that standard steel inspection forms are used for monitoring the footbridge components [9]. Inspection of the steel must be carried out carefully by a qualified person.

Inspection Procedures

Root Cause Analysis (RCA), Five-by-Five Whys (FFW) inspection techniques could be useful.

In a steel footbridge, the following components are important for inspection.

Anchorages

The anchorages will be inspected for rusting of the turnbuckles and hooks, functionality of the threads and integrity of the individual members. The anchorages are exposed to vandalism and may be adversely affected by misuse.

Steel Cables

The cables should be checked for rusting, spalling of the steel threads and general loss of tension. The loss of tension is not easily quantifiable but should be apparent from loss of structural integrity or deformation of the footbridge. Hand testing may also be used as general check for cable tautness.

Cable Connections

The live load from pedestrian traffic and wind effects tends to impose stresses on the connections. The connections may loose functionality as a result of shearing of bolts and rivets, unscrewing of nuts or slackness in grips and studs. Each joint should be examined visually for any such failures and the defects repaired.

Cable Seating

The cable seating over the deck is exposed to movement of the rope over the saddles. This movement may lead to deterioration of the saddle seating. The saddles may be moved out of position and the anchor bolts may be sheared. The movement of the cable over the saddle is enhanced by greasing the saddle seating.

Steel Deck

The steel deck is exposed to live loads from pedestrian activity. The deck may be subjected to unusual loads leading to localised failure of the deck walkway. The deck may fail if concentrated live loads are imposed. The deck is also prone to normal wear and tear from human activity leading to the wearing off of the deck connections as well as the general deterioration of the steel components. The deck should also be inspected for any signs of rusting.

Maintenance Procedures

Anchorages, Steel Cables and Cable Connections

Those steel components showing advanced rusting should be repaired by painting the parts with approved weather resistant paint or bitumen seal. The connections should be retightened where they are loose. In cases where the components are no longer functional, the connections should be replaced completely by new parts. If the cables are slack, then re-tensioning should be done by adjusting the turnbuckles, care being taken not to over tension the cables. The sag may be monitored as a check for the main cables.

Cable Seating

The bearings are greatly affected by friction generated from cable movements over the supports. The friction should be minimised by applying a lubricant, e.g., grease.

Steel Deck

The steel deck should be painted in places where advanced rusting is observed. If an individual panel has deteriorated to such an extent that it is now unsafe, then the panel should be removed and be replaced by a new one. Take care not to weaken the adjoining panels and to secure the panel correctly.

D.7.3. 6 References

[1] Melchers R.E., Hough R., Modeling complex engineering structures, Reston, Virginia: ASCE.

[2] Estes A.C., Frangopol D.M., “Updating bridge reliability based on bridge management”.

[3] Marsh P.S., Frangopol D.M., “Reinforced concrete bridge deck reliability model incorporating temporal and spatial variations of probabilistic corrosion rate sensor data,” *Reliability Engineering and System Safety*, vol. 93 , p. 394–409, 2008.

[4] Decò A., Frangopol D.M. , “Risk assessment of highway bridges under multiple hazards,” *Journal of Risk Research,* no. DOI:10.1080/13669877.2011.571789, 2011.

[5] Simiu E., Heckert N.A., Filliben J.J., Johnson S.K., “Extreme wind load estimates based on Gumbel distribution of dynamic pressures: an assessment,” *Structural Safety,* vol. 23, pp. 221-229, 2001.

[6] “CNR DT207-2008 Istruzioni per la valutazione delle azioni e degli effetti del vento sulle costruzioni, ROMA – 17 gennaio 2008”.

[7] Chiodi R., Ricciardelli F., Pelino V., Prota A.,, “Updated statistical analysis of Italian extreme wind speeds”.

[8] “UNI EN 1990, 2002 Annex B Management of Structural Reliability for Construction Works and Annex C Basis for Partial Factor Design and Reliability Analysis”.

[9] Chipuru E.V., “Guidelines for the design and construction of suspension footbridges,” International labour organization, 2000.